

Non-iterative blind deconvolution algorithm and its improvement for astronomical imaging

Maxim Usatov

Černochova 1291/4, Košice, Prague, Czech Republic

March 30, 2013

This paper presents a simple blind deconvolution algorithm and its improvement using the estimation of the modulation transfer function (MTF) for atmospheric turbulence. The improvement is optimized towards ground based astronomical imaging applications. However, it can be applied to other more generic cases that involve imaging through turbulent atmospheric layers. These algorithms are described and a number of results are obtained from a computational implementation and presented.

Introduction

Many deconvolution algorithms known today are used in a wide range of applications, including astronomy, seismology, medicine and signal processing. This paper concentrates mostly on the 2D image restoration of ground-based astronomical images. Many traditional deconvolution algorithms, such as Lucy-Richardson [1, 2] and van Cittert [3], are iterative and require substantial amounts of computing power and time to process large amounts of data. A priori knowledge of the point spread function (PSF) is also usually required in order to successfully recover the degraded input. In many applications, the PSF is unknown and this leads to the additional requirement of its estimation and fine-tuning. Certain techniques may assist in the estimation of the PSF and other unknowns. However, in many cases substantial human interaction is inevitable throughout the process of restoration. This inconvenience is further complicated by the necessity to employ many deconvolution iterations at every step.

Several methods have been proposed for blind deconvolution, which do not require a priori knowledge of the PSF and active research continues in this area. In practice, all blind deconvolution algorithms require some partial knowledge about the input or imaging process. If the blind deconvolution algorithm considered is iterative and depends on many unknowns, it is in some cases difficult to appreciate any advantages it provides compared to non-blind iterative algorithms, whereby the PSF can be estimated empirically. One such example would be ground-based telescope imaging, whereby atmospheric turbulence plays a major role in the blurring function that is approximately Gaussian-shaped. In the quest, here, for a deconvolution algorithm, Solar System imaging has been used as a test bed for a blind deconvolution algorithm that is non-iterative. Despite the number of unknowns in the blind algorithm, its results are comparable to many traditional algorithms. The advantage of getting a final result with a single iteration allows for a much more productive estimation of the blurring function.

Theory

This work takes root in the blind deconvolution algorithm proposed in [4] as described below. It is based on the assumption that the degradation function in the frequency domain is non-

negative, smooth and slowly varying. This holds true for a number of degradations occurring in various imaging applications and especially blurring by atmospheric turbulence and some lens intrinsic aberrations.

Traditional degradation theory poses that:

$$g(x, y) = f(x, y) * b(x, y) + n(x, y), \quad (1)$$

where $f(x, y)$ is the original spatial domain image, $b(x, y)$ is the PSF of the degradation, $n(x, y)$ is generally additive white noise and $*$ represents convolution. If one ignores noise for the moment, and takes the Fourier transform of equation (1), then since the degradation is assumed to be non-negative, one may represent each term of the transformed equation by its frequency domain magnitude (often called the spectrum.) Here the magnitude is defined as the square root of the sum of the squares of the real and imaginary terms in the Fourier transform. Thus one may represent equation (1) in the frequency domain as:

$$|G(\omega_1, \omega_2)| = |F(\omega_1, \omega_2)| \cdot |B(\omega_1, \omega_2)|, \quad (2)$$

where $|\dots|$ represents the magnitude of the Fourier transform

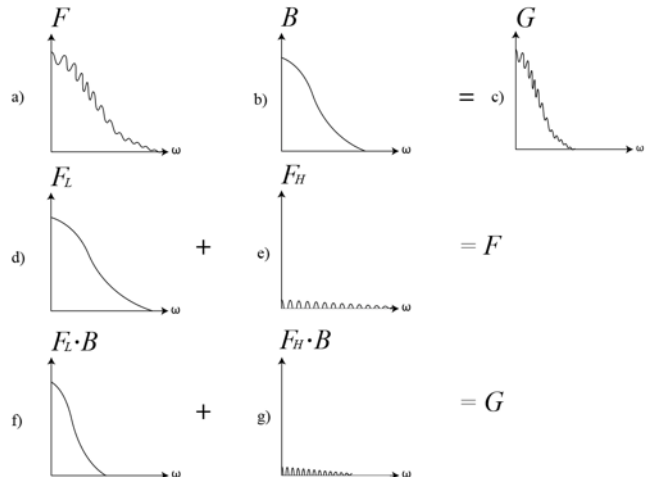


Fig 1. Development of blind deconvolution algorithm.

and \cdot represents simple multiplication. The function $|F(\omega_1, \omega_2)|$ is then assumed to be a sum of two components, a smooth lower frequency component $|F_L(\omega_1, \omega_2)|$ and a rapidly varying, higher frequency component $|F_H(\omega_1, \omega_2)|$.

Thus,

$$|F_L(\omega_1, \omega_2)| \cdot |B(\omega_1, \omega_2)| + |F_H(\omega_1, \omega_2)| \cdot |B(\omega_1, \omega_2)| = |G(\omega_1, \omega_2)|. \quad (3)$$

This is graphically shown in figure 1. If one applies a moderate linear smoothing operation S to (3), it becomes:

$$S[|F_L(\omega_1, \omega_2)| \cdot |B(\omega_1, \omega_2)|] + S[|F_H(\omega_1, \omega_2)| \cdot |B(\omega_1, \omega_2)|] = S[|G(\omega_1, \omega_2)|]. \quad (4)$$

Since both $|F_L(\omega_1, \omega_2)|$ and $|B(\omega_1, \omega_2)|$ are assumed to be smooth and slowly varying functions, a moderate smoothing operation will not affect the first term of equation (4) significantly, but will smooth away the second term. Based on this, equation (4) reduces to

$$|F_L(\omega_1, \omega_2)| \cdot |B(\omega_1, \omega_2)| \approx S[|G(\omega_1, \omega_2)|]. \quad (5)$$

By rearranging terms, equation (5) becomes:

$$|B(\omega_1, \omega_2)| \approx \frac{S[|G(\omega_1, \omega_2)|]}{|F_L(\omega_1, \omega_2)|}. \quad (6)$$

Historically, the denominator of equation (5) has been approximated by an image with similar spectral characteristics [4, 5, 6]. The downside of this approach is that the replacement image can influence the characteristics of the recovered image. For example, color shifts can occur. This problem can be mitigated, for example, by matching the histogram of the replacement image to that of the degraded image.

On the other hand, it is apparent from figure 1f and figure 1b that $S[|G(\omega_1, \omega_2)|]$ is narrower than $|B(\omega_1, \omega_2)|$. That is, the smoothed product between the slowly varying signal and the slowly varying degradation MTF is narrower than the degradation itself. For the product of two Gaussian distributions, this is a well-known fact [7]. Thus another approach is to replace the denominator in equation (6) with the degraded image smoothed even more in order to compensate for the narrowing. Thus, equation (6) becomes:

$$|B(\omega_1, \omega_2)| \approx \frac{S_1[|G(\omega_1, \omega_2)|]}{S_2[|G(\omega_1, \omega_2)|]}, \quad (7)$$

where S_2 is a broader smoothing function than S_1 . Since equation (7) has proved moderately successfully in this work, it is proposed that any transformation of the numerator in equation (6) that will effectively broaden it should also be a viable approach and permit the elimination of the denominator term. The type of function that is needed is one that amplifies high frequency components and attenuates low frequency components. In most images, the high frequency components generally have small amplitudes and low frequency components have high amplitudes. Thus, one seeks a function that attenuates

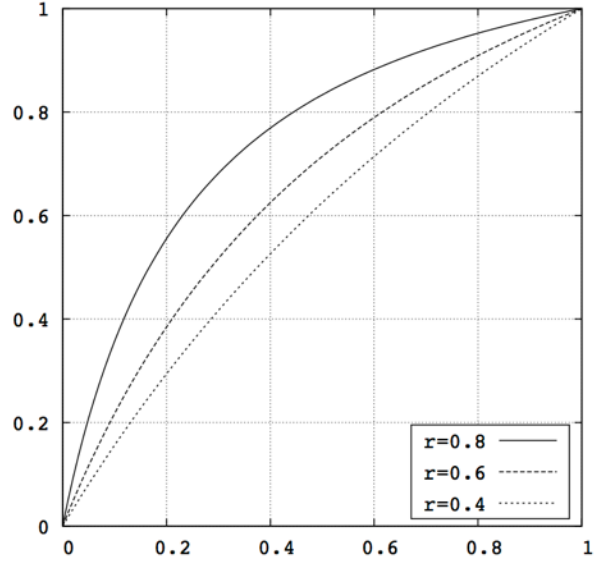


Fig 2. Graphical representation of the soft knee compressor used in equations (10) and (11) with $t = 1$.

the higher amplitudes and amplifies the lower amplitudes, thereby producing a broadening effect. Thus equation (7) becomes:

$$|B(\omega_1, \omega_2)| \approx T\{S_1[|G(\omega_1, \omega_2)|]\}, \quad (8)$$

where T is such an intensity transformation. One function that has been tested successfully in this work is a scaled logarithm such that equation (8) becomes:

$$|B(\omega_1, \omega_2)| \approx \frac{\log \{c \cdot S_1[|G(\omega_1, \omega_2)|] + 1\}}{\log (c + 1)}, \quad (9)$$

where c is a scaling constant, typically in the range of about 10 to a few hundred. The motivation for the logarithm function comes from its use in generating the cepstrum [8], where the logarithm is used for similar amplification and attenuation. Another function is a dynamic range or soft knee compressor, which has been used in the sound industry and in robot vision systems [9]. When it is applied, equation (8) becomes:

$$|B(\omega_1, \omega_2)| \approx \frac{S_1[|G(\omega_1, \omega_2)|]}{r\{S_1[|G(\omega_1, \omega_2)|] - t\} + t}, \quad (10)$$

where r is a ratio between 0 and 1. We set $t = 1$ so that the transformation range goes from 0,0 to 1,1, as shown in figure 2. The knee compressor is more symmetric than the logarithm and appears to work somewhat better. Equation (10) serves as the basis for the blind deconvolution algorithm presented in this paper. An important aspect of (10) is that it is relatively easy to compute.

Deconvolution

In order to apply the degradation function derived above, one can employ many well-known deconvolution techniques. This

includes Wiener and Constrained Least Squares (CLS) filtering [10], the iterative procedure described in [11], inverse filtering and many others. The Wiener filter is used below, although good results have also been achieved with CLS filtering. The Wiener filter serves well for the majority of image restoration tasks, since it executes an optimal tradeoff between inverse filtering and noise suppression and is generally easier to implement. The Wiener filter is expressed as following:

$$F'(\omega_1, \omega_2) = \frac{G(\omega_1, \omega_2) B^*(\omega_1, \omega_2)}{|B(\omega_1, \omega_2)|^2 + N(\omega_1, \omega_2)}, \quad (11)$$

where $F'(\omega_1, \omega_2)$ is the restored image, superscript * denotes complex conjugation and $N(\omega_1, \omega_2)$ is the noise-to-signal power spectral ratio estimate. In many image restoration cases, it is practically to substitute $N(\omega_1, \omega_2)$ with a constant, which can often be estimated from the variance of a flat region compared to the variance of the whole spatial image. An example of blind deconvolution using Wiener filtering is shown in figures 3 and 4 using equation (10) to estimate the degradation.

Improvement with atmospheric turbulence MTF

Of particular interested here is the restoration of astronomical images taken with ground-based telescopes. The degradation of such images can be attributed on the one hand to telescope intrinsic aberrations such as spherical aberration, coma, astigmatism and defocus; and on the other hand to induced aberrations, such as atmospheric turbulence, low-level turbulence and tube currents. The modulation transfer function of a majority of these aberrations is often smooth and slowly varying. It is known that atmospheric turbulence is often the largest contributor to image degradation in today's world of high quality telescope optics. The author has personally observed that including the estimated MTF of the atmospheric turbulence in equation (10) often produces better results than the blind deconvolution alone. The MTF of atmospheric turbulence can be estimated as described in [12]:

$$A(\xi) = \exp \left\{ -3.44 \left(\lambda f \frac{\xi}{r_0} \right)^{5/3} \left[1 - \alpha \left(\lambda f \frac{\xi}{D} \right)^{1/3} \right] \right\}, \quad (12)$$

where D is the entrance pupil diameter of the receiving optic (telescope), f is the focal length of the objective, λ is the wavelength, ξ is the spatial frequency, r_0 is the Fried's parameter representing the coherence parameter of the atmospheric wave front distortions and α is Fried's parameter (0 for long exposure case, 1 for short exposure case). A detailed description of Fried's atmospheric turbulence model is available in [12]. In the computational implementation employed here, a transition between the spatial frequency ξ and the normalized frequencies ω_1 and ω_2 that are used in equation (10) is implemented via a cut-off frequency based upon the linear pixel size of the CCD sensor of the imaging system. In order to get the benefit of both the blind and atmospheric MTFs, equations (10) and (12) are combined as:

$$|B_i(\omega_1, \omega_2)| \approx [|B(\omega_1, \omega_2)|]^{\gamma} \cdot [|A(\omega_1, \omega_2)|]^{(1-\gamma)}, \quad (13)$$

where $|B_i(\omega_1, \omega_2)|$ is the blurring function combining both blind and the atmospheric turbulence MTF, and γ defines the



Fig 3. Alpine Valley Rille on the Moon. Degraded image obtained by Maxim Usatov with 0.25m Maksutov-Cassegrain telescope in Prague, Czech Republic in poor seeing conditions. This is a stack of multiple frames registered and averaged with the lucky imaging approach. This image is severely degraded by atmospheric turbulence.

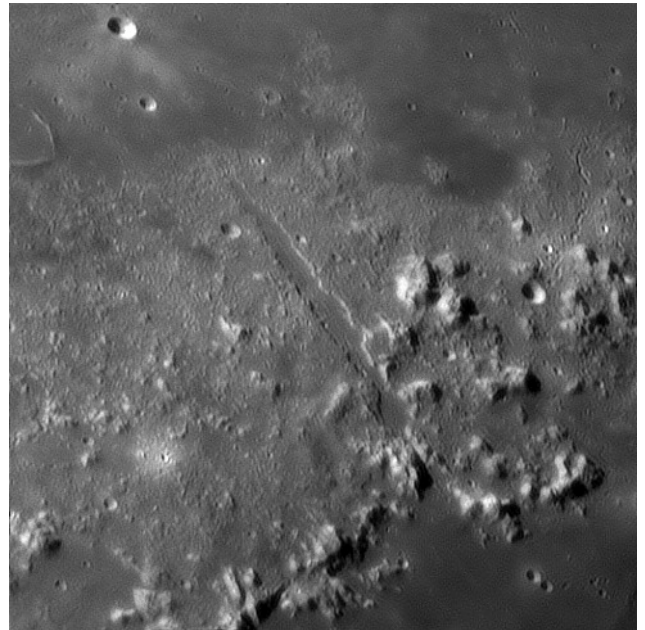


Fig 4. Alpine Valley Rille on the Moon, fig. 1 input image restored with Wiener filtering using the blind deconvolution algorithm described by equation (10). Blind deconvolution parameters used: $r=0.75$, $N=0.0006$, smoothing Gaussian weighted filter sigma of 29 pixels.

weight of blind and atmospheric components. With $\gamma = 0.5$ equation (13) forms a geometric mean between blindly estimated the blurring function $|B(\omega_1, \omega_2)|$ and the atmospheric turbulence blurring function $|A(\omega_1, \omega_2)|$. It is worth noting that

absolutely all parameters required to estimate $A(\omega_1, \omega_2)$ are known a priori except r_0 . Various methods exist for estimating r_0 , such as DIMM (Differential Image Motion Monitor). However, it is relatively easy for an experienced astronomer (even an amateur) to get a good starting point for r_0 estimation based upon the subjective quality assessment of the images obtained or by measuring the PSF of an exposed star. It is also worth noting that in the computational implementation, the author has used the so called central and separate wavelength modes to estimate the atmospheric turbulence MTF for RGB color images. In the former case a single wavelength average was used for all the channels. In the latter case, an estimate was made of each of the three MTF curves with a precise wavelength given to each channel. In the case where RGB channels of an image represent the visual spectrum range, both modes produce fine results. However, one may prefer the separate wavelength mode to process images with synthetic palettes representing broad spectrum ranges, for example, for images containing both IR and UV data in different channels. Throughout experimental testing of the improved (blended) approach in Solar System imaging applications, $\alpha = 0$ ((long exposure case) has been assumed, despite the fact that the images were obtained with short exposures. The reason for this is that the traditional practice when imaging bright objects like the planets of the Solar System and the Moon is to employ the so called “lucky imaging” approach, whereby many - hundreds or even thousands - of individual short exposure frames are taken and some percentage of the best frames are averaged together in order to produce the final image subject to deconvolution. This lucky imaging approach allows one to filter out the worst instances of degradation due to atmospheric turbulence, producing synthetic r_0 values valid for successful restoration. Lucky imaging r_0 values may exceed true r_0 measurements by a factor of four in poor seeing conditions, as shown in [13]. This is also in line with the author’s observations. A comparison between blind and improved deconvolution algorithms is shown in figures 5-8. It is clearly visible that the algorithm improved by the atmospheric turbulence MTF produces a sharper image with more contrast in the case of the Jupiter image from Pic Du Midi observatory. In some cases though, the atmospheric turbulence MTF brings little improvement to the original blind algorithm. It is believed that the improved approach works well in situations where the image has been degraded by multiple aberrations of different character, one of them being atmospheric turbulence. In the example of the Jupiter image used, turbulence plays a major part in the degradation of the images obtained. However, there were also other significant factors contributing to the blurring. In particular, Jupiter’s elevation angle for Pyreness was fairly low in September 2010 when the image was taken. So some degree of smearing in the input can be attributed to atmospheric dispersion.

Conclusions

In this paper, a simple yet efficient algorithm for restoration of signals using a non-iterative blind deconvolution approach has been presented. It works for many image restoration cases whereby the blurring function is smooth and slowly varying. Many astronomical imaging cases suffer from this kind of degradation. The algorithm is further improved by adding the MTF of atmospheric turbulence into the formula making it optimized for a wide range of astronomical applications. The

non-iterative nature of the algorithm and its computational simplicity enable convenient workflow to estimate various unknowns in a very short period of time. With the improved algorithm, a benchmark of 290 kpixels per second has been achieved on a desktop class iMac computer with 2.66 GHz Intel Core 2 Duo processor, restoring a 32-bit precision image. This results in a 1000x1000 pixels RGB image deconvolved in less than 4 seconds. Despite the fact that this paper is focused on astronomical imaging, the deconvolution algorithm presented can be used in a wide variety of other applications, for example, long range imaging, satellite imaging, aerial photography, photo radar ticketing devices, ground cameras tracking rocket launches, microscopy and many more. I would like to thank Yuri Goryachko for assisting with numerous trials of the algorithm and its modifications and helping to improve its implementation.

References

- [1] L. B. Lucy, "An iterative technique for the rectification of observed distributions," *Astronomical Journal* 79 (6): 745–754, (1974).
- [2] W. H. Richardson, "Bayesian-Based Iterative Method of Image Restoration," *JOSA* 62 (1): 55–59, (1972).
- [3] P. H. van Cittert, *ZAp*, 69, 298, (1931).
- [4] J. S. Lim, “Two-dimensional signal and image processing,” *Prentice Hall*, (1990).
- [5] J.N. Caron, N.M. Namazi, and C.J. Rollins, "Non-iterative blind data restoration by use of an extracted filter function," *Applied Optics*, Vol 41, No. 32, p. 6884, (2002).
- [6] C. D. McGillem, P.E. Anuta and K. B. Yu, "Estimation of Modulation Transfer Function of Landsat-4 Sensors from Measured Imagery," *LARS Technical Reports*. Paper 61. (1984).
- [7] P. A. Bromiley, “Products and Convolutions of Gaussian Distributions,” *Tina Memo*, No. 2003-003, (2003).
- [8] M. Cannon, “Blind deconvolution of spatially invariant image blurs with phase,” *IEEE Trans. Acoust, Speech, Signal Processing*, vol. 24(1), pp. 58-63, Feb. 1976.
- [9] Vonikakis, V., Andreadis, I., & Gasteratos, A. “Fast Dynamic Range Compression for Grey Scale Image,” *Int. Workshop on Advanced Imaging Technology*, (pp. 35-39). Bangkok, Thailand, (2007).
- [10] B. R. Hunt, “The application of constrained least squares estimation to image restoration by digital computer,” *IEEE Trans. Comput.*, Vol. C-22, pp. 805-812. (1973).
- [11] R. W. Schafer, R. M. Mersereau, and M. A. Richards, “Constrained iterative restoration algorithms,” *Proc. IEEE*, Vol. 69, pp. 432-450. (1981).
- [12] D. L. Fried, “Optical resolution through a randomly inhomogeneous medium for very long and very short exposures,” *J. Opt. Soc. Am.* 56(10), 1372-1379, (1966).
- [13] N. M Law, “Lucky imaging: diffraction-limited astronomy from the ground in the visible,” *The Observatory* 127, 71–71, (2007).

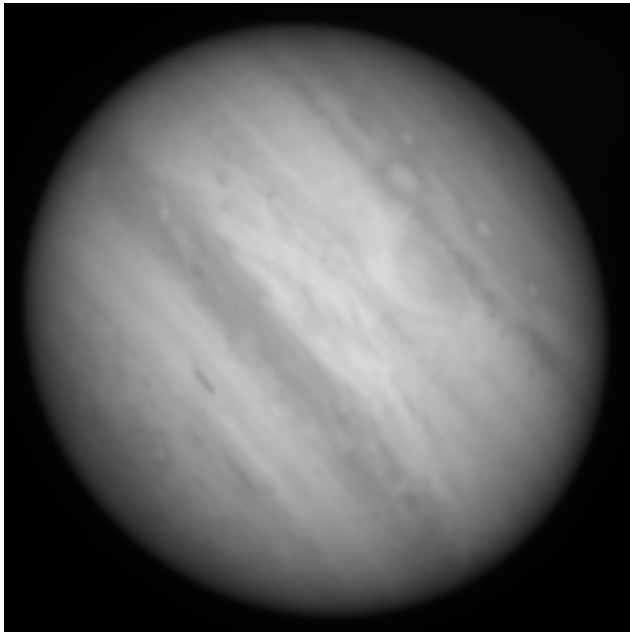


Fig 5. Jupiter image (red channel) obtained by Jean-Luc Dauvergne, Elie Rousset and Philippe Tosi with 1m Cassegrain telescope at Pic Du Midi Observatory in Pyrenees, France.

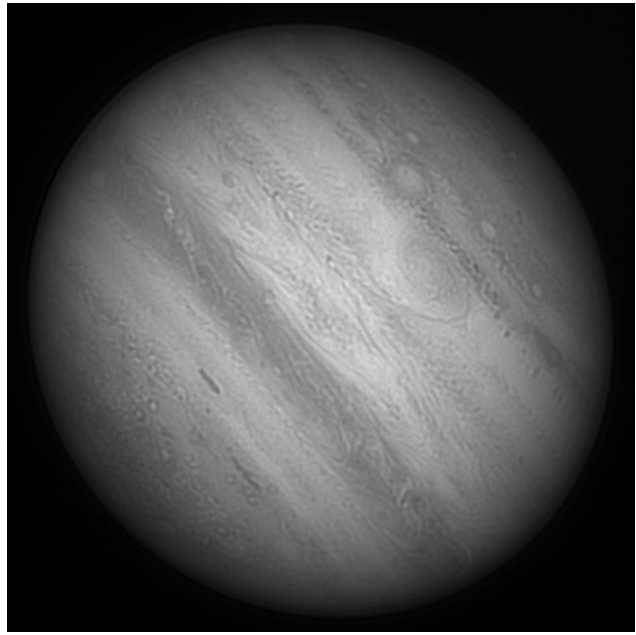


Fig 6. Jupiter input image, deconvolved using the basic blind deconvolution method.

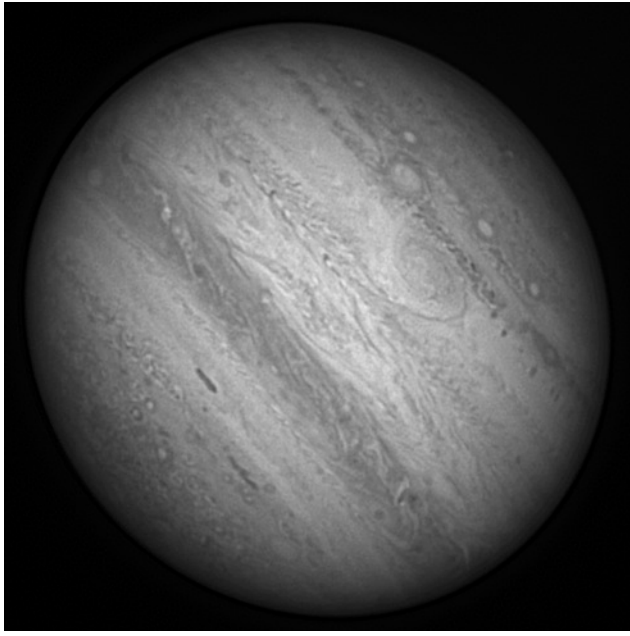


Fig 7. Jupiter input image, deconvolved using the blind algorithm improved with atmospheric turbulence MTF estimation and $\gamma = 0.5$, as per equation (13). $r_0 = 400\text{mm}$ was used (guessed) which is in line with independent imager's estimation of astronomical seeing varying 0.3 to 0.4 arcsec FWHM that corresponds to r_0 range of 360 to 480mm.

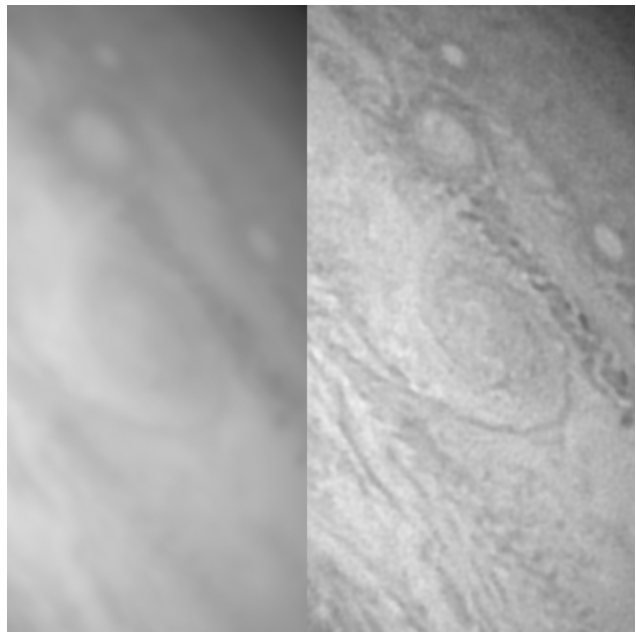


Fig 8. Jupiter input image, 100% scale, Great Red Spot feature close up comparison between the input image (left) and its deconvolved version using the blind algorithm improved with atmospheric turbulence MTF estimation.